

Solitary waves in liquid crystalline waveguides

Miroslaw A. Karpierz

Faculty of Physics, Warsaw University of Technology, Koszykowa 75, 00-662 Warszawa, Poland

(Received 27 March 2002; published 6 September 2002)

Recently, it has been shown experimentally that the nonlinearity in nematic liquid crystals can govern spatial solitons in both waveguide and bulk geometry. Such solitons require a few milliwatts of light power and can be controlled by the state of light polarization or by an external electrical field. In this paper a detailed theoretical analysis of optical solitary waves in nematic liquid crystal waveguides is presented. The self-focusing is induced by reorientation nonlinearity in the homeotropically aligned nematic layer. This configuration corresponds to the experimental setup in which we previously observed such solitary waves. The theoretical results presented in this paper correlate exactly with the experiments.

DOI: 10.1103/PhysRevE.66.036603

PACS number(s): 42.65.Wi, 42.70.Df

I. INTRODUCTION

Liquid crystals are materials with many unique physical, optical, and electro-optical properties. New compounds and mixtures of liquid crystals are chemically stable, with low absorption, very large optical anisotropy, a liquid crystalline phase in a wide range of temperatures, are easily oriented at boundaries, and are also easily reoriented by electrical or magnetic fields. Therefore, they are important optical materials for numerous applications in modern optoelectronics [1].

Liquid crystals are also an excellent medium for nonlinear optics [1–3]. The main contribution to nonlinear optical phenomena in liquid crystals arises from thermal and reorientation processes. While the thermal effect is similar to that observed in other materials, the reorientation effect is characteristic only of a liquid crystalline phase. The nonlinearity due to the reorientation effect in a nematic phase leads to numerous effects not observed in any other types of nonlinearity. The reorientation nonlinearity induces extremely large nonlinear changes in the value of the refractive index that can be obtained using relatively low light power. This nonlinearity depends on both boundary conditions and geometry of the system and can be easily modified by external electrical or magnetic fields. This type of nonlinearity depends on light polarization but, within a wide range, is independent of light wavelengths. The main drawback is slow response time but, by special optimization of the system, this response could be fairly fast.

Nonlinear optics of liquid crystals has been a subject of intensive study for more than twenty years. Most of the theoretical and experimental work has been done for thin samples and only a few papers reported nonlinear propagation of light beams at distances greater than the Rayleigh distance [4]. There have been experiments showing self-focusing due to the reorientation process inside liquid crystals in capillaries [5–7], planar cells [8,9], and planar waveguides [10].

In this paper the self-focusing effect due to the reorientation nonlinearity in a planar waveguide filled with homeotropically aligned nematic liquid crystal is analyzed (see Fig. 1) [11–13]. The analyzed configuration corresponds to the experimental geometry in which solitary waves were observed

[10]. In the homeotropic texture, liquid crystalline molecules are perpendicular to the bounded plates (parallel to the x coordinate) and are forced to rotate into the orientation which is parallel to the electrical field of the light wave. Therefore the electromagnetic wave with TM polarization (with E_x component of the electrical field) does not induce any reorientation. On the other hand, the TE-polarized wave (with E_y component of the electrical field) could induce a large reorientation.

When the electrical field tends to reorient liquid crystalline molecules positioned at an angle of $\pi/2$, the reorientation starts above the threshold value of the electrical field. This phenomenon is called the Freedericksz threshold transition. The origin of this effect is the fact that torque-rotating liquid crystal molecules do not exist for electrical fields perpendicular to the anisotropic molecules. The reorientation can start due to fluctuations in the molecular orientation, but it requires a sufficiently strong electrical field. For intensities above the threshold level, the reorientation rise very fast with increasing light intensity. The resulting nonlinear increasing of the refractive index is very large due to the large birefringence of nematic liquid crystals. However, experimentally observed self-focusing in the presence of the Freedericksz threshold showed undulation, filamentation, and break-up of the light beam [5,7,10]. The stable spatial solitons were measured when the nonlinear reorientation were very weak and without threshold [8–10]. The reorientation nonlinearity is saturable and nonlocal, which generally stabilizes self-focusing and creation of robust spatial solitons [14]. In such media an unstable propagation could also appear [15,16] especially when the nonlinear changes of refractive index are large and the light beam significantly deviates from the soliton shape and width. From that point of view the self-

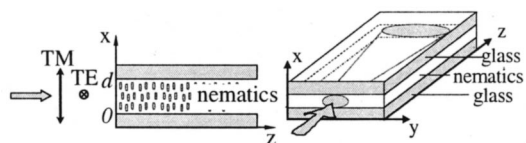


FIG. 1. Schematic drawing of liquid crystalline planar waveguides.

focusing of pure TE-like fields in analyzed structures could be unstable.

The theoretical analysis in this paper is limited to stationary solutions corresponding to the experimentally observed stable beams. Therefore, the light beam with both TM and TE fields, but with a stronger TM-like component, will be considered. Consequently, the nonlinear effects will start without a threshold and the reorientation will be very small. These assumptions allow us to use a low-nonlinearity approximation, where the electromagnetic field in the direction perpendicular to the film is not changed by the nonlinearity, i.e., its distribution is the same as in a planar waveguide with the initial orientation of the nematic liquid crystal. As a result the analysis is simplified by reduction to 1+1 dimensions.

II. BEAM PROPAGATION IN ANISOTROPIC WAVEGUIDES

Liquid crystals are anisotropic materials with an anisotropy axis connected with molecular orientation. Assuming that possible changes in the orientation of liquid crystals take place in the xy plane, the electrical permittivity tensor has the form

$$\epsilon = \begin{pmatrix} \epsilon_{\perp} + \Delta\epsilon \cos^2\theta & \Delta\epsilon \cos\theta \sin\theta & 0 \\ \Delta\epsilon \cos\theta \sin\theta & \epsilon_{\perp} + \Delta\epsilon \sin^2\theta & 0 \\ 0 & 0 & \epsilon_{\perp} \end{pmatrix}. \quad (1)$$

In Eq. (1) $\Delta\epsilon = \epsilon_{\parallel} - \epsilon_{\perp}$ represents an optical anisotropy, $\epsilon_{\perp} = n_o^2$ is an ordinary electrical permittivity, $\epsilon_{\parallel} = n_e^2$ is an extraordinary one, and θ is an orientation angle of the liquid crystalline molecules measured according to the x axis. In such a medium the Maxwell equations for the monochromatic electromagnetic wave have the form

$$\left[k_0^2 \epsilon_{yy} + \frac{\partial^2}{\partial x^2} + \frac{\partial^2}{\partial y^2} \frac{\epsilon_{yy}}{\epsilon_{zz}} + \frac{\partial^2}{\partial z^2} + \frac{\partial^2}{\partial x \partial y} \frac{\epsilon_{xy}}{\epsilon_{zz}} \right] E_y = \left[-k_0^2 \epsilon_{xy} - \frac{\partial^2}{\partial y^2} \frac{\epsilon_{xy}}{\epsilon_{zz}} - \frac{\partial^2}{\partial x \partial y} \left(\frac{\epsilon_{xx}}{\epsilon_{zz}} - 1 \right) \right] E_x, \quad (2)$$

$$\left[k_0^2 \epsilon_{xx} + \frac{\partial^2}{\partial x^2} \frac{\epsilon_{xx}}{\epsilon_{zz}} + \frac{\partial^2}{\partial y^2} + \frac{\partial^2}{\partial z^2} + \frac{\partial^2}{\partial x \partial y} \frac{\epsilon_{xy}}{\epsilon_{zz}} \right] E_x = \left[-k_0^2 \epsilon_{xy} - \frac{\partial^2}{\partial x^2} \frac{\epsilon_{xy}}{\epsilon_{zz}} - \frac{\partial^2}{\partial x \partial y} \left(\frac{\epsilon_{yy}}{\epsilon_{zz}} - 1 \right) \right] E_y, \quad (3)$$

where ϵ_{ab} are the components of the permittivity tensor (1) and $k_0 = \omega/c$ is the wave number.

The TE-like field is assumed to be much weaker than the TM-like field. Therefore, the reorientation of the liquid crystals and resulting electrical permittivity changes are small enough to use a small nonlinearity approximation, i.e., to use an electrical field in the form

$$E_x = A(y, z) \psi(x) \exp(i\omega t - ik_0 N_x z), \quad (4)$$

$$E_y = B(y, z) \varphi(x) \exp(i\omega t - ik_0 N_y z), \quad (5)$$

where $\psi(x) \exp(i\omega t - ik_0 N_x z)$ and $\varphi(x) \exp(i\omega t - ik_0 N_y z)$ are modes of the planar waveguide (TM and TE, respectively) with homeotropically aligned liquid crystals (for $\theta=0$), where N_x, N_y are effective refractive indices, and where A and B are complex amplitudes slowly varying with respect to z . The modes in the homeotropically-aligned liquid crystal layer fulfil the equations

$$\left[k_0^2 (\epsilon_{\parallel} - N_x^2) + \frac{\epsilon_{\parallel}}{\epsilon_{\perp}} \frac{\partial^2}{\partial x^2} \right] \psi = 0, \quad (6)$$

$$\left[k_0^2 (\epsilon_{\perp} - N_y^2) + \frac{\partial^2}{\partial x^2} \right] \varphi = 0, \quad (7)$$

and therefore have the form

$$\psi = \Psi_0 \cos \left[k_0 \xi_x \left(x - \frac{d}{2} \right) \right], \quad (8)$$

$$\varphi = \Phi_0 \cos \left[k_0 \xi_y \left(x - \frac{d}{2} \right) \right], \quad (9)$$

where Ψ_0 and Φ_0 are normalizing amplitudes

$$\xi_x = \frac{n_o}{n_e} \sqrt{n_e^2 - N_x^2}, \quad (10)$$

$$\xi_y = \sqrt{n_o^2 - N_y^2}, \quad (11)$$

and effective refractive indices are found from the dispersion relations

$$\tan \left(\frac{1}{2} k_0 \xi_{x,y} d \right) = \frac{\eta_{x,y}}{\xi_{x,y}}, \quad (12)$$

where

$$\eta_{x,y} = \sqrt{N_{x,y}^2 - n_c^2}. \quad (13)$$

Assuming that the field distributions ψ and φ as well as the reorientation angle θ distribution are symmetrical, the slowly varying complex amplitudes A and B satisfy equations obtained as a result of integration of Eqs. (2), (3) over the cross section

$$\left[\kappa_1 + \frac{1}{2k_0 N_y} \frac{\partial^2}{\partial y^2} \left(\frac{2N_y \kappa_1}{\epsilon_{\perp} k_0} + 1 \right) - i \frac{\partial}{\partial z} \right] B = \left[-\kappa_{12} - \frac{\partial^2}{\partial y^2} \frac{\kappa_{12}}{\epsilon_{\perp} k_0^2} \right] A \exp[-ik_0(N_x - N_y)z], \quad (14)$$

$$\left[-\kappa_2 + \frac{1}{2k_0 N_x} \frac{\partial^2}{\partial y^2} - i \frac{\partial}{\partial z} \right] A = [-\kappa_{21} - \delta] B \exp[ik_0(N_x - N_y)z], \quad (15)$$

where nonlinear coefficients are defined as follows:

$$\kappa_1 = \frac{k_0 \Delta \epsilon \int \varphi^2 \sin^2 \theta dx}{2N_y \int \varphi^2 dx}, \quad (16)$$

$$\kappa_2 = \frac{k_0 N_x \Delta \epsilon \int \psi^2 \sin^2 \theta dx}{2\epsilon_{\parallel} \int \psi^2 dx}, \quad (17)$$

$$\kappa_{12} = \frac{k_0 \Delta \epsilon \int \varphi \psi \sin \theta \cos \theta dx}{2N_y \int \varphi^2 dx}, \quad (18)$$

$$\kappa_{21} = \frac{k_0 \Delta \epsilon \int \varphi \psi \sin \theta \cos \theta dx}{2N_x \int \psi^2 dx}, \quad (19)$$

and

$$\delta = \frac{\Delta \epsilon \int \psi [\partial^2 (\varphi \sin 2\theta) / \partial x^2] dx}{4k_0 \epsilon_{\perp} N_x \int \psi^2 dx}. \quad (20)$$

For waveguides thicker than the wavelength $d \gg \lambda$, the coefficient δ can be neglected because it is much smaller than the coefficient κ_{21} ($\delta \ll \kappa_{21}$). Assuming that the light beam is wider than the wavelength and that the reorientation is small, components $\partial^2 \kappa_1 / \partial y^2$ and $\partial^2 \kappa_{12} / \partial y^2$ in Eq. (14) can also be neglected. Consequently, the set of Eqs. (14), (15) is reduced to the simpler form

$$\left[\kappa_1 + \frac{1}{2k_0 N_y} \frac{\partial^2}{\partial y^2} - i \frac{\partial}{\partial z} \right] B = -\kappa_{12} A \exp[-ik_0(N_x - N_y)z], \quad (21)$$

$$\left[-\kappa_2 + \frac{1}{2k_0 N_x} \frac{\partial^2}{\partial y^2} - i \frac{\partial}{\partial z} \right] A = -\kappa_{21} B \exp[ik_0(N_x - N_y)z]. \quad (22)$$

Additionally, using the normalized modes, the number of nonlinear coefficients is reduced: $\kappa_{12} \approx \kappa_{21}$ and $\kappa_1 \approx \kappa_2$. For the small reorientation, $\kappa_{12} \gg \kappa_1$ and κ_1 can also be disregarded. Reorientation increases the effective index for the TE-like field while the effective index for the TM-like field is decreased. Therefore, the nonlinear coefficients κ_1 and κ_2 have different signs in Eqs. (21) and (22).

III. REORIENTATION NONLINEARITY

At a given temperature, nematic liquid crystal molecules fluctuate around the mean direction defined by the director \mathbf{n} . The distortion of the molecular alignment corresponds to the free energy density [1–3]

$$f_F = \frac{K_1}{2} (\nabla \mathbf{n})^2 + \frac{K_2}{2} (\mathbf{n} \cdot \nabla \times \mathbf{n})^2 + \frac{K_3}{2} (\mathbf{n} \times \nabla \times \mathbf{n})^2, \quad (23)$$

where K_i represents elastic constants for three different basic deformations splay ($i=1$), twist ($i=2$), and bend ($i=3$). Usually $K_3 > K_1 > K_2$, but equations are simplified by assuming the one-elastic constant approximation $K_1 \approx K_2 \approx K_3 = K$.

External electrical or magnetic fields create a torque on the molecules and change the orientation of the liquid crystal. For optical frequencies the interaction with the magnetic field is insignificant and the light wave interaction with the nematic liquid crystals is caused by the electrical field. The orientation-dependent term in the energy density of interaction between the electrical field and liquid crystal molecules is equal to

$$f_{\text{opt}} = -\frac{\epsilon_0 \Delta \epsilon}{2} \langle (\mathbf{n} \cdot \mathbf{E})^2 \rangle. \quad (24)$$

The total free energy density composed of deformation energy f_F and interaction energy f_{opt} fulfils a minimization procedure. The orientation angle θ (between the director \mathbf{n} and the x axis) is sufficient to describe molecular reorientation limited to two dimensions. The Euler-Lagrange equation takes the form

$$\frac{\partial}{\partial x} \frac{\partial (f_F + f_{\text{opt}})}{\partial \left(\frac{d\theta}{dx} \right)} - \frac{\partial (f_F + f_{\text{opt}})}{\partial \theta} = 0, \quad (25)$$

where both energy densities (23) and (24) are described using the orientation angle, because $\mathbf{n} = (\cos \theta, \sin \theta, 0)$. Consequently, for the one-elastic constant approximation (with the assumption of equal energies for splay and bend deformations), the orientation angle θ is calculated from the Euler-Lagrange equation in the form

$$\frac{4K}{\epsilon_0 \Delta \epsilon} \frac{d^2 \theta}{dx^2} + 2|AB| \psi \varphi \cos \Delta \alpha \cos 2\theta + (|B\varphi|^2 - |A\psi|^2) \sin 2\theta = 0, \quad (26)$$

where $\Delta \alpha$ is the difference of phases between E_x and E_y field components. The solution of Eq. (26) requires satisfying the boundary conditions which, for strong anchoring and initial homeotropic alignment, are equal to $\theta(0) = \theta(d) = 0$.

In Fig. 2 the dependence of nonlinear coefficients κ_{12} , κ_1 , and κ_2 on light power is shown. The value of these coefficients was calculated using the definitions (16)–(18) for reorientation obtained directly from Eq. (26) for the field distribution defined by Eqs. (8) and (9). The numerical results were calculated for the waveguide made by a liquid crystal film of the thickness $d = 10 \mu\text{m}$ with refractive indices $n_o = 1.52$ and $n_e = 1.69$, surrounded by glass plates with the refractive index $n_c = 1.45$ and for the wavelength $\lambda = 842 \text{ nm}$. The values of refractive indices correspond to the 4-*trans*-4'-*n*-hexyl-cyclohexyl-isothiocyantobenzene (6CHBT) nematic liquid crystal. The power density of the

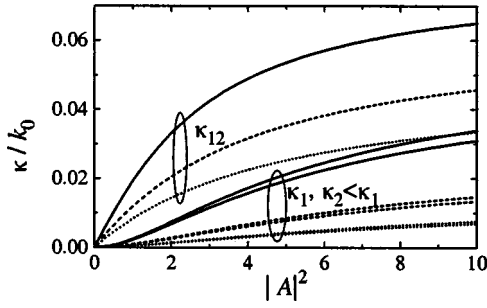


FIG. 2. Dependence of nonlinear parameters κ_{12} , κ_1 , and κ_2 on light power density in the TM mode for different values of amplitude ratios: solid line for $|B/A|=0.5$, dashed line for $|B/A|=0.2$, and dotted line for $|B/A|=0.1$. Both components of the field were in the same phase (i.e., $\Delta\alpha=0$).

guided fundamental mode is characterized by a dimensionless value of $|A|^2$, obtained under the assumption that the field distributions are normalized as

$$N_y \int \varphi^2(x) dx = N_x \int \psi^2(x) dx = \frac{4K}{\epsilon_0 \Delta \epsilon d}. \quad (27)$$

For a typical value of the elastic constant $K \approx 10^{-11}$ N (as in the 6CHBT liquid crystal), the dimensionless power $|A|^2 = 1$ corresponds to the power density $P \approx 2$ mW/ μm .

Introducing an angle β defined as

$$\tan 2\beta = \frac{2|AB|\psi\varphi \cos \Delta\alpha}{|A\psi|^2 - |B\varphi|^2}, \quad (28)$$

Eq. (26) can be rewritten in the form

$$\frac{d^2\theta}{dx^2} - \frac{\sigma^2}{2} \sin 2(\theta - \beta) = 0, \quad (29)$$

where

$$\sigma^2 = \frac{\epsilon_0 \Delta \epsilon}{2K} \sqrt{(|A\psi|^2 - |B\varphi|^2)^2 + (2|AB|\psi\varphi \cos \Delta\alpha)^2}. \quad (30)$$

The analytical solution of Eq. (29) exists for homogeneous distribution of the electrical field $\psi = \varphi = \text{const}$ (i.e., for $\varphi^2 = \psi^2 = 4K/\epsilon_0 \Delta \epsilon d^2$). In this case, for boundary conditions $\theta(0) = \theta(d) = 0$, the distribution of the orientation angle θ is described as

$$\sin\left(\theta - \beta + \frac{\pi}{2}\right) = \sqrt{m} \text{sn}[\sigma(x + x_0)|m], \quad (31)$$

where $\text{sn}(u|m)$ is the Jacobian elliptic function with modulus m [17]. The integration constant x_0 for given boundary conditions is equal to

$$x_0 = \frac{2K(m) - \sigma d}{2\sigma}, \quad (32)$$

where $K(m)$ is the complete elliptic integral.

Using the boundary condition $\theta(0) = 0$ in Eq. (31), the following relation is obtained:

$$\cos \beta = \sqrt{m} \frac{\text{cn}(\sigma d/2|m)}{\text{dn}(\sigma d/2|m)}, \quad (33)$$

where $\text{cn}(u|m)$ and $\text{dn}(u|m)$ are Jacobian elliptic functions. Equation (33) can be used to calculate the value of the modulus m . In the case of small values of electrical field intensity (small values of $u = \sigma d/2$), the ratio of elliptic function can be expanded into the series $[\text{dn}(u|m)/\text{cn}(u|m)]^2 \approx 1 + (1-m)u^2 + \dots$. Consequently, from Eq. (33) the following formula is obtained:

$$m \approx \frac{1 + u^2}{1 + \tan^2 \beta + u^2}. \quad (34)$$

The modulus m of the Jacobian elliptic function is connected with the maximal angle of reorientation in the center of the liquid crystalline layer $\theta_{\text{max}} = \theta(d/2)$:

$$m = \cos^2(\beta - \theta_{\text{max}}). \quad (35)$$

For a small reorientation angle $\theta_{\text{max}} < \beta \ll 1$ it can be assumed that $m \approx 1 - \beta^2 + 2\theta_{\text{max}}\beta$ and $\tan \beta \approx \beta$. Using Eq. (34) the maximal reorientation angle has the following approximate value:

$$\theta_{\text{max}} \approx \frac{1}{2} \beta \frac{\beta^2 + u^2}{1 + \beta^2 + u^2}. \quad (36)$$

Because of the condition $|A| \gg |B|$, it can be additionally assumed—using definitions (28) and (30)—that $\beta \approx |AB| \cos \Delta\alpha / (|A|^2 - |B|^2)$ and $u^2 + \beta^2 \approx (|A|^2 - |B|^2)/2$, and consequently,

$$\theta_{\text{max}} \approx \frac{1}{4} \frac{|AB| \cos \Delta\alpha}{1 + (|A|^2 - |B|^2)/2}. \quad (37)$$

The maximal values of reorientation in Eq. (37) were calculated for homogeneous distribution of the electrical field across the liquid crystalline sample. However it can be expected that, in the case where $\psi(x)$ and $\varphi(x)$ describe modal field distributions [Eqs. (8) and (9)], the dependence of maximal reorientation on electrical field amplitude is similar to that of Eq. (37). Therefore, the maximal reorientation angle should be proportional to the parameter

$$R = \frac{|AB| \cos \Delta\alpha}{1 + (|A|^2 - |B|^2)/A_S^2}, \quad (38)$$

where the value of saturation amplitude A_S can be estimated for a given waveguide. Consequently, the nonlinear coefficients κ_{12} , κ_1 , and κ_2 are expected to be proportional to R and R^2 [see definitions (16)–(18)]. The accuracy of such an estimate is shown in Fig. 3(a), where the dependence of nonlinear parameters κ_{12} , $\sqrt{\kappa_1}$, and $\sqrt{\kappa_2}$ on parameter R is plotted. The saturation amplitude $A_S^2 = 5.44$ used in Fig. 3(a) has

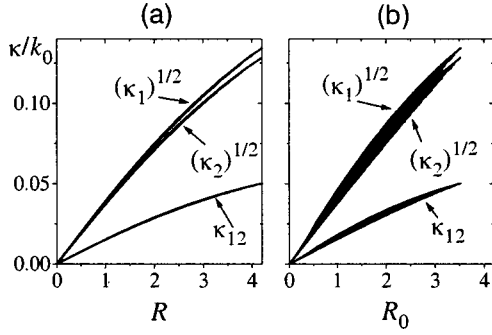


FIG. 3. Dependence of nonlinear parameters κ_{12} , $(\kappa_1)^{1/2}$, and $(\kappa_2)^{1/2}$ on (a) the parameter R and (b) the simplified parameter R_0 . Each curve is composed of 100 lines obtained for different values of amplitudes $|A|^2 \in (0,10)$ and $|B|^2 \in (0,0.25|A|^2)$, and for different phase differences $\Delta\alpha \in (0, \pi/2)$.

been estimated from the dependence of κ_{12} on field intensity in the case $|B|^2 = 0.01|A|^2$ and $\Delta\alpha = 0$, where $|A|^2 \in (0,10)$ (dotted curve presented in Fig. 2). In Fig. 3(a) one hundred lines for each coefficient were plotted. They were obtained for the field parameters varying in the following ranges: $\Delta\alpha \in (0, \pi/2)$, $|A|^2 \in (0,10)$, and $|B|^2 \in (0, |A|^2/4)$. As can be seen, the parameter R linearizes the coefficients κ_{12} and $\sqrt{\kappa_p}$ ($p=1,2$) with a very high accuracy. To compare this approximation with another, the dependence of coefficients κ_{12} , $\sqrt{\kappa_1}$, and $\sqrt{\kappa_2}$ on the simplified parameter

$$R_0 = \frac{|AB| \cos \Delta\alpha}{1 + |A|^2/A_S^2} \quad (39)$$

is presented in Fig. 3(b). In this case the parameter R_0 seems to be useful only for a very small reorientation, i.e., for $R_0 \ll 1$.

In general, the analyzed nonlinearity depends on $|AB| \cos \Delta\alpha$ and is saturated with respect to $|A|^2 - |B|^2$ (or in low nonlinearity with respect to $|A|^2$). Therefore the nonlinearity can also be approximated with reasonable accuracy by the exponential function

$$R_{\text{exp}} = \frac{|AB| \cos \Delta\alpha}{|A|^2 - |B|^2} \left[1 - \exp\left(-\frac{|A|^2 - |B|^2}{A_S^2}\right) \right] \quad (40)$$

(with $A_S^2 = 4.31$ for the analyzed waveguide) or a generalized model of the saturation nonlinearity

$$R_{\text{sat}} = \frac{|AB| \cos \Delta\alpha}{|A|^2 - |B|^2} \left[1 - \left(1 + \frac{|A|^2 - |B|^2}{A_S^2}\right)^{-s} \right] \quad (41)$$

(with $A_S^2 = 5.57$ and $s = 1.03$ for the analyzed waveguide). However, in this paper the form of nonlinearity dependent on R defined by Eq. (38) will be used. Consequently, both nonlinear parameters will have the form

$$\kappa_{12} = \kappa_0 \frac{2|AB| \cos \Delta\alpha}{1 + (|A|^2 - |B|^2)/A_S^2}, \quad (42)$$

$$\kappa_2 \approx \kappa_1 = \kappa_{10} \frac{4|AB|^2 \cos^2 \Delta\alpha}{[1 + (|A|^2 - |B|^2)/A_S^2]^2}, \quad (43)$$

with $\kappa_0 = 0.007k_0$ and $\kappa_{10} = 0.0003k_0$ for the analyzed waveguide.

IV. APPROXIMATE SOLUTION FOR SOLITARY WAVES

The propagation of light beams in homeotropically oriented liquid crystalline waveguides is described by Eqs. (21), (22) with nonlinear coefficients in the approximate forms (42), (43). This set of equations requires numerical analysis but in this section some simplified solutions will be presented. First, because $\kappa_1 \approx \kappa_2 \ll \kappa_{12}$, the nonlinear coefficients κ_1 and κ_2 will be eliminated. Second, components with dense oscillating terms $\exp\{\pm i[k_0(N_x - N_y)z + \Delta\alpha]\}$ will be removed from Eqs. (21),(22). Subsequently, the equations describing beam propagation in analyzed waveguides take the form

$$i \frac{\partial B}{\partial z} = \frac{1}{2k_0 N_y} \frac{\partial^2 B}{\partial y^2} + \frac{\kappa_0 |A|^2 B}{1 + (|A|^2 - |B|^2)/A_S^2}, \quad (44)$$

$$i \frac{\partial A}{\partial z} = \frac{1}{2k_0 N_x} \frac{\partial^2 A}{\partial y^2} + \frac{\kappa_0 |B|^2 A}{1 + (|A|^2 - |B|^2)/A_S^2}. \quad (45)$$

Equations (44),(45) are similar to equations describing vectorial solitons in media with saturable nonlinearity [18]. The difference is that, in contrast to typical saturable nonlinearity, there exists only a nonlinear cross-phase modulation saturated by a difference of field intensities $|A|^2 - |B|^2$.

In searching for the spatial soliton solution it is convenient to introduce the ansatz

$$B(y,z) = \frac{u(y)}{\sqrt{2k_0 N_x \kappa_0}} \exp\left(\frac{-ipz}{2k_0 N_y}\right), \quad (46)$$

$$A(y,z) = \frac{w(y)}{\sqrt{2k_0 N_y \kappa_0}} \exp\left(\frac{-iqz}{2k_0 N_x}\right), \quad (47)$$

with real amplitudes u, w and real parameters p, q . Therefore Eqs. (44),(45) can be rewritten in the form

$$\frac{d^2 u}{dy^2} - pu + \frac{w^2 u}{1 + \gamma(N_x w^2 - N_y u^2)} = 0, \quad (48)$$

$$\frac{d^2 w}{dy^2} - qw + \frac{u^2 w}{1 + \gamma(N_x w^2 - N_y u^2)} = 0, \quad (49)$$

where $\gamma = (2k_0 N_x N_y \kappa_0 A_S^2)^{-1}$. Only solutions in the form of bright solitons will be examined, i.e., the solutions with $w(y \rightarrow \pm\infty) = u(y \rightarrow \pm\infty) = 0$ and $(d/dy)w(y=0) = (d/dy)u(y=0) = 0$.

In the case of $N_x w^2 = N_y u^2$ the saturation disappears and, consequently, the solution of Eqs. (48),(49) is

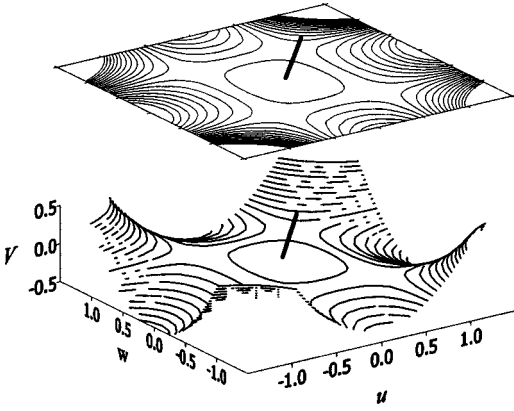


FIG. 4. Plot of potential V , defined by Eq. (53), for parameters $p=0.5$ and $q=0.3$. The thick solid line shows the trajectory matched to given boundary conditions.

$$w(y) = \frac{w_0}{\cosh(w_0 y / \sqrt{2})}, \quad (50)$$

where $w_0^2 = 2N_x p = 2N_y q$.

The saturation effectively decreases the nonlinear effect and causes the soliton to be wider. The relative changes in soliton width and shape are not so significantly modified by the term of saturation. Therefore, it can be expected that the solution obtained for nonsaturable nonlinearity will be sufficient to predict properties of solitons in saturable nonlinear media.

The solution of Eqs. (48), (49) consists of a complicated problem which requires matching parameters p and q with given boundary conditions. However, in nonsaturable media ($\gamma=0$) the set of equations is simplified to

$$\frac{d^2 u}{dy^2} - pu + w^2 u = 0, \quad (51)$$

$$\frac{d^2 w}{dy^2} - qw + u^2 w = 0. \quad (52)$$

Equations (51), (52) are identical to equations describing the two-dimensional motion of a particle in the potential V :

$$V(u, w) = \frac{1}{2}(u^2 w^2 - pu^2 - qw^2), \quad (53)$$

where u and w are generalized positions, y represents time, and du/dy , dw/dy are momenta. The potential surface for parameters $p=0.5$ and $q=0.3$ is presented in Fig. 4. The thick solid line shows the trajectory fulfilling the boundary conditions such as $w=u=0$ and $dw/dy=du/dy=0$ for $y \rightarrow \pm\infty$. Such conditions require the trajectory in the uw plane to be limited between the points $(u, w) = (0, 0)$ and (u_0, w_0) , with the same potential $V(u_0, w_0) = V(0, 0) = 0$. The point (u_0, w_0) corresponds to the soliton center $u_0 = u(0)$, $w_0 = w(0)$ because it satisfies the condition $dw/dy = du/dy = 0$. The analogy with the mechanical system (proposed in Ref. [19]) allows us to calculate the integral of

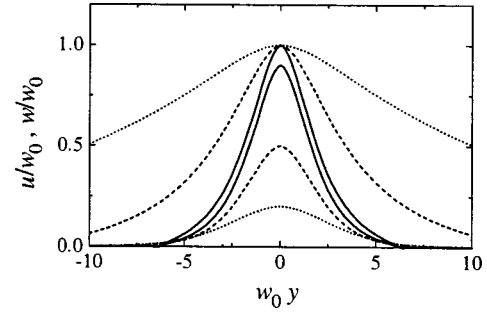


FIG. 5. Soliton amplitude distributions in both polarization components for different amplitude ratios: solid line for $w_0/u_0=1.1$, dashed line for $w_0/u_0=2$, and dotted line for $w_0/u_0=5$. Upper curves correspond to the distribution of $w(y)/w_0$ while lower curves correspond to $u(y)/w_0$.

motion (total energy), which is useful in determining the relationship between parameters p , q and amplitudes in the soliton center w_0 , u_0 :

$$\frac{p}{w_0^2} + \frac{q}{u_0^2} = 1. \quad (54)$$

Next, the solution of Eqs. (51), (52) requires matching only one of the parameters q or p with given values of amplitudes w_0 and u_0 . In Fig. 5 shapes of solitary beams are presented at different ratios of amplitudes in the beam center w_0/u_0 . For a given ratio w_0/u_0 , the width of the beam is proportional to the inverse of beam amplitude because the soliton solution can be transformed into a new one according to the relation

$$u(y) = u_0 f(w_0 y), \quad (55)$$

$$w(y) = w_0 g(u_0 y). \quad (56)$$

The widths of both beam components u and w are different. The beam widths at a half amplitude σ_w and σ_u [where $w(\sigma_w) = w_0/2$ and $u(\sigma_u) = u_0/2$] depend on the ratio w_0/u_0 , as presented in Fig. 6. From a numerical calculation it can be estimated that the ratio of widths of both beam polarizations is roughly a linear function of the amplitudes ratio as

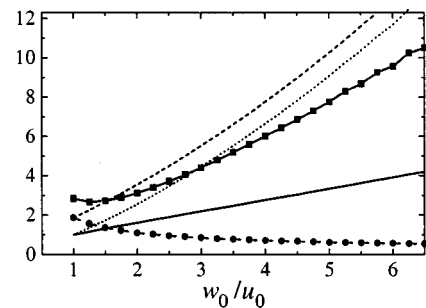


FIG. 6. Dependence on the ratio of amplitude values at the beam center w_0/u_0 : beam component widths $\sigma_w w_0$ (dashed line) and $\sigma_u u_0$ (dashed line with circles), the ratio of these widths σ_w/σ_u (solid line), the square root of power ratio $(\pi_w/\pi_u)^{1/2}$ (dotted line), and the total power $(\pi_w + \pi_u)/w_0$ (solid line with squares).

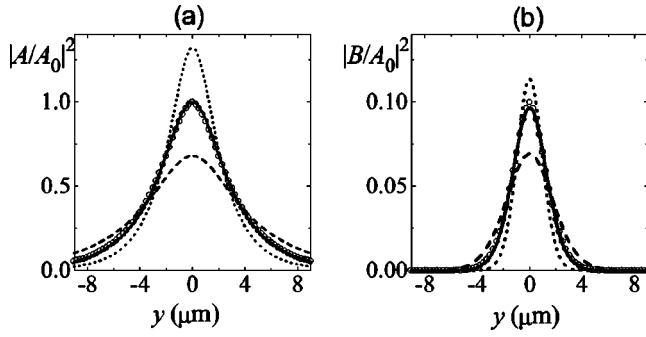


FIG. 7. Beam intensity distribution (a) for the TM component and (b) for the TE component on the input plane (represented by solid line with circles) and at the distance $z=1150 \mu\text{m}$ for different inputs: dashed line for $A_0^2=1$, solid line for $A_0^2=1.5$, and dotted line for $A_0^2=3$.

follows: $\sigma_w/\sigma_u \approx 0.4 + 0.6w_0/u_0$. The dependence of normalized beam power in both beam components is also presented in Fig. 6. The power of the beam components is represented by quantities $\pi_w = \int w^2 dy$ and $\pi_u = \int u^2 dy$, respectively. It should be noted that the ratio of energies grows faster than the ratio of maximal intensities of both beam components. This is caused by the fact that, by increasing the ratio of amplitudes, the ratio of relative widths of both polarization components also increases. The existence of the TE component is necessary to induce the self-focusing of the TM-polarized beam. When the TM beam is very wide the self-focusing term, which compensates for the diffraction, could be weak, and the TE component could be narrow and with a low power. On the other hand, for a narrow TM component the diffraction is strong and the creation of solitary waves requires high nonlinearity. Consequently, for a narrow TM component the inducing nonlinearity TE component should be relatively wider, and with higher power than that for the wide TM component.

V. NUMERICAL RESULTS

Equations (21), (22) with nonlinear coefficients (42), (43) can be solved by using numerical beam propagation methods (BPM's). Results presented in this section were obtained with an application of the finite difference BPM for waveguide parameters (the same as used in Sec. III). First, the accuracy of the solutions of the approximate Eqs. (51), (52) is presented below. Assuming that the beam launched to the waveguide has an amplitude ratio of $|A(y=0)/B(y=0)|^2 = 10$, corresponding to $w_0/u_0 \approx 3.0$, one can find from the approximate solution that $\sigma_w w_0 \approx 5.5$ and $\sigma_w/\sigma_u \approx 2.2$, i.e., the TM component of the solitary wave is more than twice the width of the TE component. Consequently, when the light beam has the sizes $\sigma_w = 5.0 \mu\text{m}$ and $\sigma_u \approx 2.3 \mu\text{m}$, the solitary wave should be formed for $A(y=0) = A_0 \approx 1.0$. The Rayleigh distance, defined as $z_R = \pi N \sigma^2 / \lambda \ln 2$, for such a beam is $z_R \approx 230 \mu\text{m}$ for the TM component and $z_R \approx 40 \mu\text{m}$ for the TE component, respectively.

In Fig. 7 we present amplitude shapes at the distance of $z=1150 \mu\text{m}$. This distance corresponds to 5 Rayleigh dis-

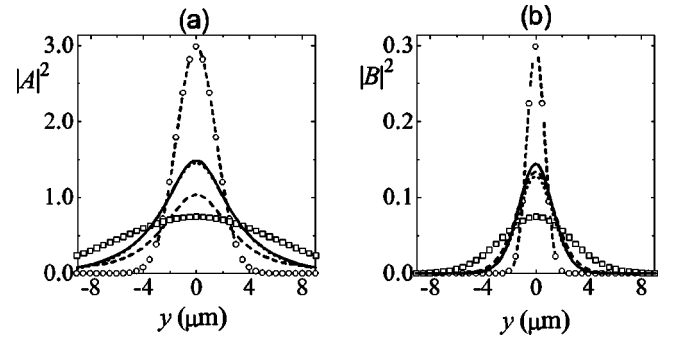


FIG. 8. Beam intensity distribution on the input plane (represented by lines with open circles and open squares) and at the distance $z=1150 \mu\text{m}$, for input beams with the same power but different widths: dashed line for Gaussian input $A^2(y=0, z=0) = 2A_0^2$, dotted line for Gaussian input $A^2(y=0, z=0) = 0.5A_0^2$, and solid line for solitary wave $A^2(y=0, z=0) = A_0^2 = 1.5$.

tances for the wider TM beam component and to more than 26 Rayleigh distances for the TE beam component. As is shown by the dashed line in Fig. 7, the beam which is the solution of Eqs. (51), (52) is not strictly a solitary wave. The beam over a long distance takes a solitary wave form which is wider and has a lower intensity than the input beam represented by the solid line with circles in Fig. 7. However, for an intensity of 1.5 times larger than the input beam, i.e., for $A_0^2 \approx 1.5$, the shape and intensity of the input is almost the same as in the solitary wave formed at long distances (solid line in Fig. 7). For larger amplitudes, solitary waves are narrower than the input beam (dotted line in Fig. 7 for $A_0^2 = 3$). The differences between an exact and an approximate solution are caused mainly by the absence of saturation of the nonlinearity. For solitary beams corresponding to higher intensities (with values of intensity closer to the saturation A_S^2), the differences are larger. However, the shape of the solitary wave obtained by solving the simplified equations (51), (52) seems to be a very good approximation, more accurate than the Gaussian or sech functions and much simpler to calculate than the exact solution.

The propagation of analyzed solitary waves is stable, and beams adjust to the nearest solitary shape and amplitude. Because light in both orthogonal polarizations has different phase velocities, the exchange of energy between both polarization components is irrelevant. Therefore, the beam tends to adjust to the form appropriate for the initial ratio of energy in both polarization components. Of course, if the input beam deviates too much from the solitary wave, some amount of energy radiates out and the beam adjusts to the solitary wave existing at a lower level of power. The shape of solitary waves formed at large distances for inputs with different shapes but with the same energy ratio between TM and TE components is shown in Fig. 8. The dotted line in Fig. 8 represents the solitary wave formed by the beam which on the input plane is twice as wide and has an intensity twice as low as the solitary wave represented by the solid line in Fig. 8. Conversely, the dashed line in Fig. 8 represents the solitary wave formed by the beam which on the input plane is twice as narrow and has an intensity twice

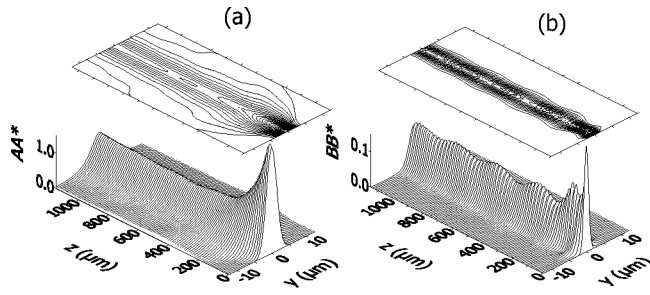


FIG. 9. Distribution of light intensity in (a) TM component and (b) TE component of the beam along the propagation distance for the solitary beam, shown as a solid line in Figs. 7 and 8.

as high as the solitary wave represented by the solid line in Fig. 8. Both beams create nondiffracted solitary waves with very similar amplitudes. In the case of narrower input (dashed line in Fig. 8), some amount of energy is radiated out as presented in Fig. 9. As a result, the solitary wave has an energy ratio which is lower than the ratio in the input beam. When the width of both beam polarization components is the same on the input plane, the beam also adjusts to the nearest form of solitary wave. This behavior is presented in Fig. 10, obtained for the Gaussian input with the same widths of both polarization components and with an energy ratio corresponding to that of Figs. 8 and 9.

Self-focusing phenomena in analyzed waveguides are caused by reorientation of liquid crystalline molecules. The reorientation is largest for the linearly polarized light, that is, when both TE and TM components are in the same phase or when they are in opposite phases (the direction of reorientation is different in both cases). On the other hand, for the phase differences $\Delta\alpha = \pm\pi/4$, reorientation does not occur at all because in this case, the long axis of the polarization ellipse is parallel to the alignment of liquid crystalline molecules. Both TE and TM components of the light beam have different phase velocities. Therefore, the reorientation is periodic, following changes in beam polarization. The changes in the coefficient κ_{12} along the propagation distance are presented in Fig. 11. These changes, presented in Fig. 11, were obtained for a solitary wave in the same way as in Fig. 8 for

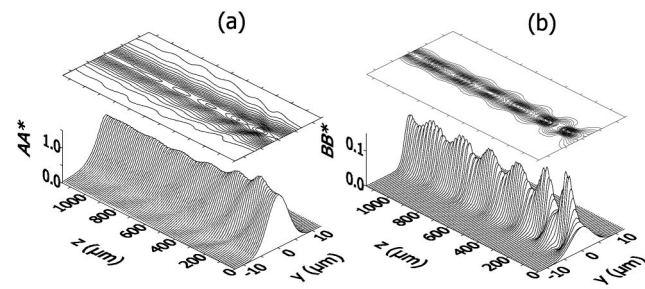


FIG. 10. Distribution of light intensity of the beam along the propagation distance for the input Gaussian beam with the same widths for both polarization components. The width of the TM component corresponds to the proper solitary solution while the width of the TE component is approximately twice as large as that of the solitary wave.

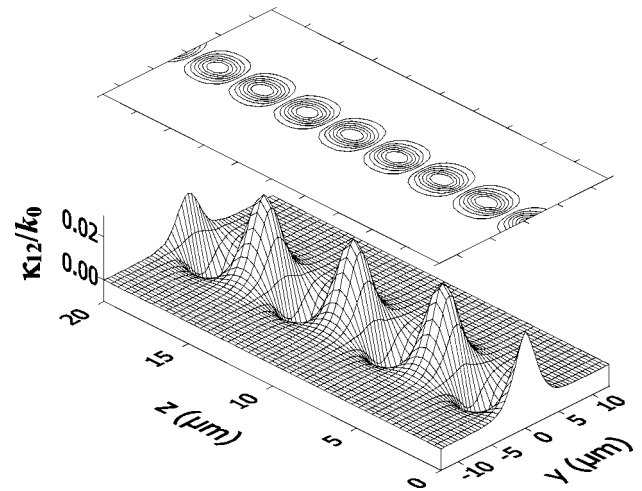


FIG. 11. Distribution of the nonlinear coefficient κ_{12}/k_0 in the region of solitary wave propagation.

$A_0^2 = 1.5$ (and in the following figures), starting from the plane $z=0$, where both polarization components share the same phase. The coefficient κ_{12} represents an effective reorientation and its sign corresponds to the direction of the molecular rotation. The period of reorientation is equal to the polarization beat length $L_B = \lambda/(N_x - N_y)$ and for analyzed waveguide $L_B \approx 5 \mu\text{m}$. The width of the region where reorientation takes place is the same as the width of the TE wave component.

Periodic reorientation causes the amplitude of the solitary waves to oscillate. These oscillations are greater for beams with higher power because of larger reorientation. Periodic reorientation is also responsible for the behavior during the collision of two beams: periodic reorientation induced by one beam acts as gratings where the second beam is scattering. Therefore, the solitary waves obtained in the analyzed geometry of liquid crystalline waveguides are not strictly solitons because they are modified or even destroyed due to interaction with other beams [20]. Collisions of two solitary waves are presented in Figs. 12 and 13. When both beams have the same phase, they collapse and create one solitary beam. This new beam has lower power, because some light is scattered (Fig. 12). Such behavior occurs for collisions at small angles or for parallel beams. During collisions at larger angles both beams could be completely destroyed and no solitary wave is formed after the collision. However, when

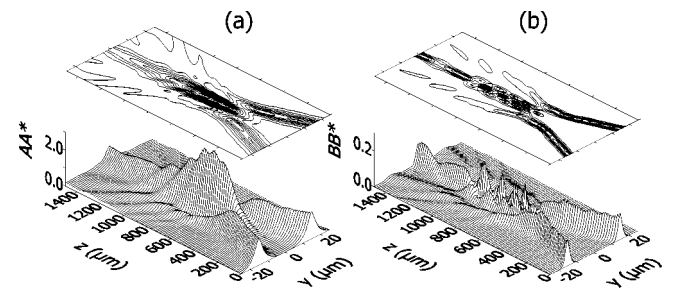


FIG. 12. Collision of two solitary waves with the same phase on the input plane.

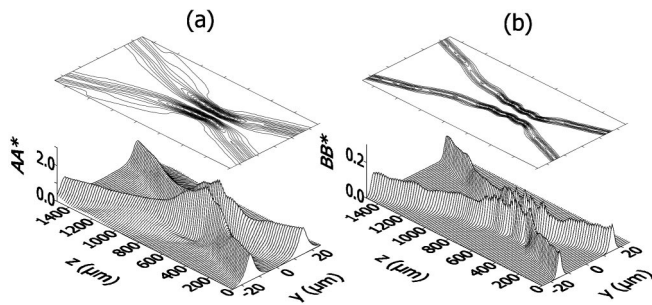


FIG. 13. Collision of two solitary waves with opposite phases on the input plane.

the angle of collision is large enough, the colliding beams behave as solitons. This is caused by the fact that the interaction length in this case is too short to significantly disturb propagating beams. When both beams have opposite phases they are repulsed as in Fig. 13, but the light also scatters and beams can also be destroyed.

VI. CONCLUSIONS

Analyzed solitary waves have been investigated experimentally in homeotropically aligned 6CHBT nematics placed between glass plates separated by $10\ \mu\text{m}$ spacers [10]. Nonlinear effects were observed for light power larger than 20 mW in the beam with a diameter of $10\ \mu\text{m}$. For TE-polarized beams the nonlinear reorientation was so strong that, after initial focusing, the beam broke up. However, for the input beam with a polarization close to the TM polarization, solitary waves were measured. The value of the light power $P \approx 30\ \text{mW}$, which was necessary to obtain the soli-

tary wave, thoroughly agrees with theoretically calculated power.

The origin of the nonlinear phenomena in liquid crystals has a different mechanism, but reorientation and thermal effects are the most significant sources of nonlinearity. The thermal effect is connected with changes in both order parameter and density of the liquid crystals, which change refractive indices and birefringence of the medium. These changes are dependent only on light intensity. On the other hand, the reorientation effect changes the orientation of the birefringence axis and is dependent on both light intensity and light polarization. The source of self-focusing in the experiment was investigated by detecting a white light passing perpendicularly through the waveguide placed between crossed polarizers. The period and size of the observed reorientation perfectly match the calculated pattern shown in Fig. 11. Therefore, the reorientation effect seems to be the main source of the creation of the observed solitary wave.

In conclusion, one should say that the liquid crystalline waveguides are media suitable for creation of spatial solitary waves. In homeotropically aligned nematic layers, solitary waves can be observed for light with a power of milliwatts. The nonlinear properties of such waveguides and of solitary waves differ from those in previously analyzed materials. Reorientation nonlinearity can be effectively described as a saturation nonlinearity dependent on light polarization. Solitary waves governed by such nonlinearity are vectorial solitons with different sizes and amplitudes for both polarization components. The reorientation connected with solitary waves is periodic, which induces scattering of light during the collisions of two solitary waves. The detailed theoretical analysis presented in this paper agrees with previously measured experimental results.

-
- [1] I. C. Khoo and S. T. Wu, *Optics and Nonlinear Optics of Liquid Crystals* (World Scientific, London, 1993).
- [2] I. C. Khoo, in *Progress in Optics XXVI*, edited by E. Wolf (Elsevier Science Amsterdam, 1988), p. 105.
- [3] N.V. Tabiryan, A.V. Sukhov, and B.Ya. Zeldovich, *Mol. Cryst. Liq. Cryst.* **136**, 1 (1986).
- [4] M. A. Karpierz, in *Soliton-driven Photonics*, edited by A. D. Boardman and A. P. Sukhorukov (Kluwer Academic, Dordrecht, 2001), p. 41.
- [5] E. Braun, L.P. Faucheux, A. Libchaber, D.W. McLaughlin, D.J. Muraki, and M.J. Shelley, *Europhys. Lett.* **23**, 239 (1993); E. Braun, L.P. Faucheux, and A. Libchaber, *Phys. Rev. A* **48**, 611 (1993).
- [6] D.W. McLaughlin, D.J. Muraki, M.J. Shelley, and X. Wang, *Physica D* **88**, 55 (1995); **97**, 471 (1996).
- [7] M. Warengem, J.F. Henninot, and G. Abbate, *Opt. Express* **2**, 483 (1998); *Mol. Cryst. Liq. Cryst.* **320**, 207 (1998).
- [8] M. Peccianti, A. De Rossi, G. Assanto, A. De Luca, C. Umeton, and I.C. Khoo, *Appl. Phys. Lett.* **77**, 7 (2000).
- [9] M. Peccianti and G. Assanto, *Opt. Lett.* **26**, 1690 (2001); **26**, 1791 (2001); *Phys. Rev. E* **65**, 035603 (2002).
- [10] M.A. Karpierz, M. Sierakowski, M. Swillo, and T.R. Wolinski, *Mol. Cryst. Liq. Cryst.* **320**, 157 (1998).
- [11] G. Abbate, F. Castaldo, and L. De Stefano, *Mol. Cryst. Liq. Cryst.* **282**, 269 (1996).
- [12] M. A. Karpierz, A. W. Domanski, M. Sierakowski, M. Swillo, and T. R. Wolinski, *Acta Phys. Pol.* **95**, 783 (1999).
- [13] C. Garcia-Reimbert, C. Garza-Hume, A.A. Minzoni, J.A. Reyes, R.F. Rodriguez, and N.S. Smyth, *Physica D* **145**, 144 (2000).
- [14] A.W. Snyder, D.J. Mitchell, and Y.S. Kivshar, *Mod. Phys. Lett. B* **9**, 1479 (1995); D.J. Mitchell and A.W. Snyder, *J. Opt. Soc. Am. B* **16**, 236 (1999).
- [15] W. Krolikowski, O. Bang, J.J. Rasmussen, and J. Wyller, *Phys. Rev. E* **64**, 016612 (2001).
- [16] M.L. Dowell, B.D. Paul, A. Gallagher, and J. Cooper, *Phys. Rev. A* **52**, 3244 (1995); M.L. Dowell, R.C. Hart, A. Gallagher, and J. Cooper, *ibid.* **53**, 1775 (1996).
- [17] P. F. Byrd and M. D. Friedman, *Handbook of Elliptic Integrals for Engineers and Scientists* (Springer Verlag, New York, 1971).
- [18] S. Gatz and J. Hermann, *J. Opt. Soc. Am. B* **8**, 2296 (1991).
- [19] A.V. Buryak and Y.S. Kivshar, *Opt. Lett.* **20**, 1612 (1994).
- [20] M.A. Karpierz and Q.V. Nguyen, *Opto-Electron. Rev.* **10**, 59 (2002).